How to cite: *Angew. Chem. Int. Ed.* **2021**, *60*, 8882–8888
International Edition: doi.org/10.1002/anie.202014711
German Edition: doi.org/10.1002/ange.202014711

VIP **Fuel Cells** ***Very Important Paper***

Platinum Dissolution in Realistic Fuel Cell Catalyst Layers

Konrad Ehelebe, Julius Knöppel, Markus Bierling, Britta Mayerhöfer, Thomas Böhm, Nadiia Kulyk, Simon Thiele, Karl J. J. Mayrhofer, and Serhiy Cherevko**

Abstract: *Pt dissolution has already been intensively studied in aqueous model systems and many mechanistic insights have been gained. Nevertheless, transfer of new knowledge to real-world fuel cell systems is still a significant challenge. To close this gap, we present a novel in situ method combining a gas diffusion electrode (GDE) half-cell with inductively coupled plasma mass spectrometry (ICP-MS). With this setup, Pt dissolution in realistic catalyst layers and the transport of dissolved Pt species through Nafion membranes were evaluated directly. We observed that 1) specific Pt dissolution increased significantly with decreasing Pt loading, 2) in comparison to experiments on aqueous model systems with flow cells, the measured dissolution in GDE experiments was considerably lower, and 3) by adding a membrane onto the catalyst layer, Pt dissolution was reduced even further. All these phenomena are attributed to the varying mass transport conditions of dissolved Pt species, influencing re-deposition and equilibrium potential.*

Introduction

Proton exchange membrane fuel cells (PEMFC) with Pt-group metal (PGM) catalysts have already reached commercialization level.[1] However, cost and durability remain the two main obstacles towards broad implementation of PEMFC-based power systems.[2] Therefore, extensive research on Pt/C electrode stability has been conducted, resulting in a series of excellent reviews in the field.[2,3] Pt dissolution and carbon corrosion have been revealed as the primary degradation mechanisms. They can initiate secondary degradation processes such as Ostwald ripening, particle migration, agglomeration and particle detachment.[3b] All those mechanisms lead to a decrease in the electrochemically active surface area (ECSA), which typically results in a lower electrode activity and therefore power losses in the PEMFC.

Different techniques have been developed to evaluate the degradation mechanisms in both aqueous electrolytes and membrane electrode assemblies (MEAs).[4] While investigations in aqueous electrolytes enable fundamental insights into degradation mechanisms, derivations to more realistic and complex MEA systems remain challenging.[5] Therefore, more applied systems that are closer to technical cell design to evaluate catalyst degradation are required.[4a,6] In contrast to the secondary degradation mechanisms which have already been evaluated well in realistic environments of MEAs, Pt dissolution mechanisms are difficult to reveal in single cell experiments, as reliable online measurements are not (yet) feasible. However, Pt dissolution has been widely studied in aqueous model systems. Especially the development of electrochemical cells coupled to inductively coupled plasma mass spectrometry (ICP-MS) enabling online evaluation of catalyst dissolution opened the door for various important insights on the dissolution mechanism.[7] The impact of various parameters—ranging from catalyst characteristics (crystal structure, particle size), catalyst layer properties (catalyst support, Pt-support-ratio, loading) and operating conditions (potential limits, sweep rate, temperature, electrolyte)—on Pt dissolution was investigated with those setups. Thereby important fundamental insights into intrinsic Pt dissolution have been revealed. The readers are referred to dedicated reviews on Pt dissolution[6b,c] and electrochemical online ICP-MS electrocatalyst research[8] for more details.

Besides intrinsic catalyst dissolution, the mass transport of dissolved Pt species away from the electrode into the electrolyte also plays a crucial role in net Pt dissolution mainly by influencing the re-deposition of dissolved Pt species.[9] Early rotating disk electrode (RDE) experiments with ex-situ ICP-MS stated a minor impact of catalyst loading on Pt dissolution.[10] Nevertheless, in recent flow cell experiments it was observed that increasing the catalyst loading leads to decreasing specific (normalized to active surface area) Pt dissolution.[6c,11] This phenomenon can be explained by the increased length of diffusion pathways for dissolved Pt species out of a thicker catalyst layer into the bulk solution. Therefore, the probability that the Pt ions remain trapped in the porous catalyst support increases. As a consequence, (i) re-deposition of dissolved Pt species is enhanced compared to Pt dissolution and (ii) a higher concentration of dissolved Pt species in the pores causes a shift in the equilibrium potential

[*] K. Ehelebe, J. Knöppel, M. Bierling, B. Mayerhöfer, T. Böhm, Dr. N. Kulyk, Prof. Dr. S. Thiele, Prof. Dr. K. J. J. Mayrhofer, Dr. S. Cherevko
Helmholtz-Institute Erlangen-Nürnberg for Renewable Energy (IEK-11), Forschungszentrum Jülich GmbH
91058 Erlangen (Germany)
E-mail: k.ehelebe@fz-juelich.de
s.cherevko@fz-juelich.de
K. Ehelebe, J. Knöppel, M. Bierling, B. Mayerhöfer, T. Böhm, Prof. Dr. S. Thiele, Prof. Dr. K. J. J. Mayrhofer
Department of Chemical and Biological Engineering
Friedrich-Alexander University Erlangen-Nürnberg
Egerlandstr. 3, 91058 Erlangen (Germany)
Supporting information and the ORCID identification number(s) for the author(s) of this article can be found under: https://doi.org/10.1002/anie.202014711.

(Nernst equation).[11] Nevertheless, it has to be noted that this phenomenon has yet mainly been investigated in model systems with very low catalyst loadings. Hitherto, only a few studies on the loading dependent degradation in MEAs have been conducted.[12] Although in these single cell experiments the contribution of the various degradation mechanisms could not be deconvoluted, enhanced degradation with decreasing Pt loading is confirmed in those studies.

Besides the Pt mass transport within the catalyst layer, mass transport out of the catalyst layer into the bulk solution is a critical factor for net Pt dissolution as well. From RDE experiments Nagai et al.[10] revealed that Pt dissolution is enhanced with increasing rotation rate. At higher rotation rates, the diffusion layer thickness and therefore transport resistance decrease, leading to facilitated mass transport of dissolved Pt species away from the electrode and decreasing re-deposition of Pt. These findings have been confirmed by Gilbert et al.[5a] who indirectly measured catalyst dissolution via in-operando small-angle X-ray scattering (SAXS) and compared catalyst degradation in aqueous (stagnant and flowing) and solid electrolyte (MEA). Further, via identical location transmission electron microscopy (IL-TEM) Nikkuni et al. found that degradation processes are less severe using a solid compared to a liquid electrolyte. They hypothesized this to be caused by a decreased mobility of dissolved species in Nafion.[13] All those studies exhibit that the mass transport of dissolved Pt species in the catalyst layer and the electrode–electrolyte interface has a major impact on the examined Pt dissolution. However, this mass transport of dissolved species can be very different in real-world systems and aqueous model systems. Therefore, understanding this phenomenon will help to unravel the significant differences in catalyst stability which have been observed in aqueous half-cells and realistic single cells.[6c,14]

Gas diffusion electrode (GDE) half-cell setups have been proposed as a suitable tool to bridge the gap between fundamental electrochemical catalyst evaluation and applied fuel cell research.[15] In this work, we extend this method for fundamental catalyst dissolution studies. Coupling a GDE half-cell[15d,16] to an ICP-MS (Figure 1) we—for the first time reported in the literature—describe time-resolved and direct measurements of Pt dissolution in realistic catalyst layers and through Nafion membranes. With this novel technique, the impact of catalyst loading and Nafion membrane thickness on Pt dissolution in GDEs is investigated. Thereby, new insights into the mobility of Pt ions within Nafion and its impact on Pt dissolution could be revealed. More detailed information on the setup and the experimental procedure can be found in the Supporting Information, Figures S1–S3.

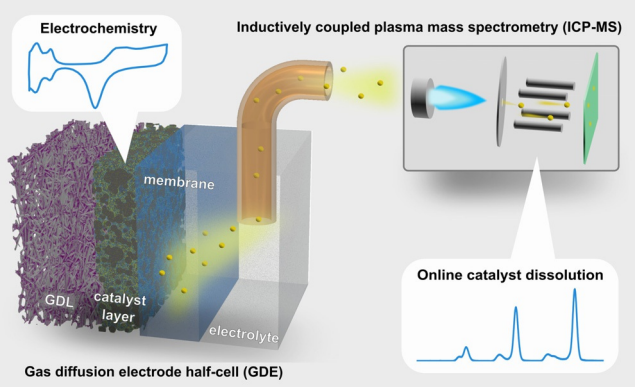

Figure 1. Scheme of the novel gas diffusion electrode (GDE) half-cell setup coupled to an inductively coupled plasma mass spectrometer (ICP-MS) used in the current work to detect catalyst dissolution.

Results and Discussion

When aiming at ultra-low Pt loadings for PEMFC, it is crucial to discuss the impact of the catalyst loading on Pt dissolution. Previous works in this field[10,11,17] have always been conducted on model surfaces. Realistic catalyst layers on gas diffusion layers (GDL) with relevant loadings for fuel cell applications have not yet been directly investigated. Figure 2 shows the impact of catalyst loading on the dissolution of Pt in realistic catalyst layers studied with the novel GDE-ICP-MS setup. The corresponding additional structural characterization and electrochemical data can be found in Figures S4–S8.

In general, from Figure 2 A–F, it can clearly be seen that specific dissolution increases with lower catalyst loading. These results match the findings of the catalyst dissolution studies on model systems conducted using scanning flow cell (SFC) experiments.[6c,11] The phenomenon has been explained by hindered mass transport of dissolved Pt species in thicker catalyst layers. This leads to impeded Pt ion mass transport away from the electrode. Therefore, re-deposition of dissolved Pt species is facilitated and effective dissolution of Pt decreased. Furthermore, the higher concentration of dissolved Pt species close to the catalyst surface lowers the dissolution rate based on thermodynamics (Le Chatelier's principle, Nernst equation).[11]

In addition to the impact of loading, some general characteristic features for Pt dissolution can be detected in the dissolution profiles measured with online GDE-ICP-MS. (i) Pt dissolution at the first slow CVs is much higher compared to subsequent CVs after 40 degradation cycles (Figure 2 B,E). This could be attributed to initial dissolution of low-coordination sites on fresh samples.[7f,18] (ii) Upon slow potential cycling, firstly a smaller dissolution peak is observed on the positive-going potential scan, followed by a significantly higher second dissolution peak during the negative-going potential scan (Figure 2 G). As already revealed in earlier online ICP-MS studies, the peaks can be ascribed to anodic dissolution due to Pt-oxide formation and cathodic dissolution due to Pt-oxide reduction, respectively. Quantitatively, cathodic dissolution clearly exceeds anodic dissolution[6b,7c,19] (iii) Nevertheless, it can also be observed that anodic dissolution is more drastically decreased after fast cycling compared to cathodic dissolution (Figure 2 G), which can again be explained with the initial (pre-dominantly anodic) dissolution occurring at undercoordinated sites during the first CVs.[7f,18b] From (ii) and (iii), it can be concluded that during unprotected start-up and shut-down events in fuel cells ($\geq$1.5 V vs. RHE[20]), cathodic dissolution is the more

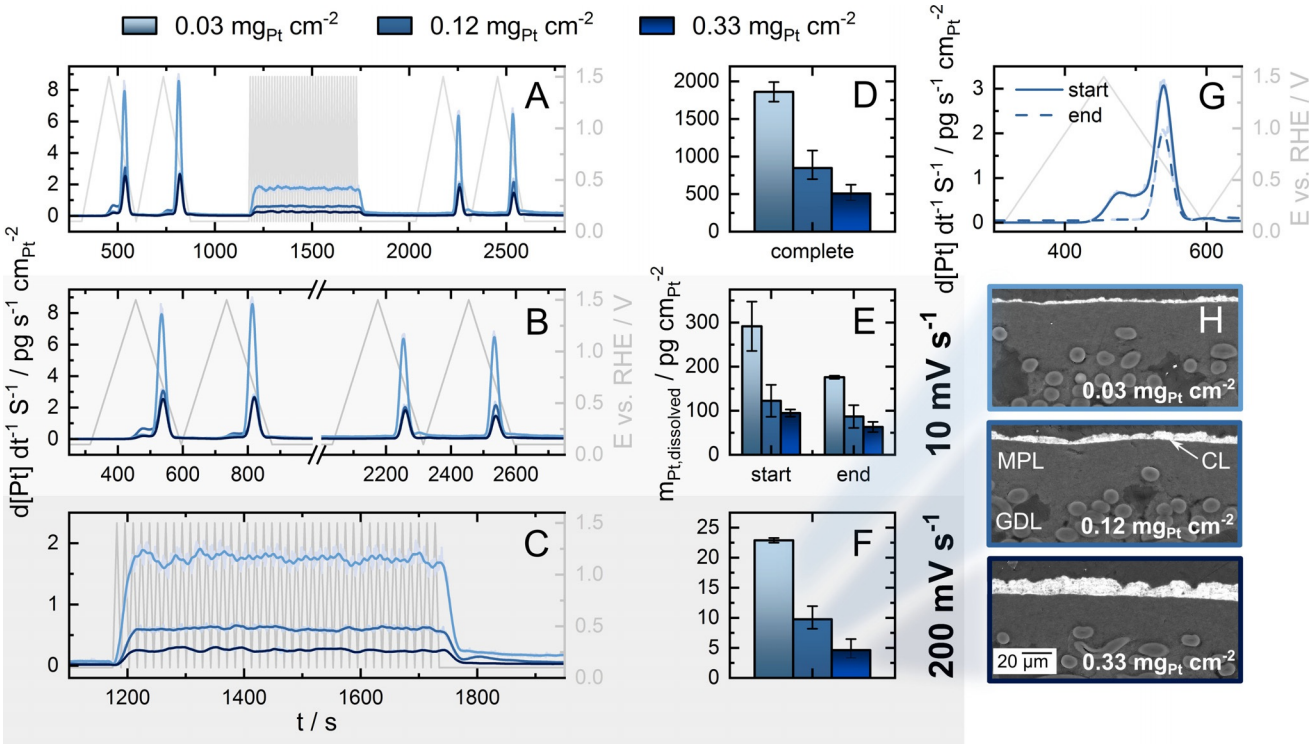

Figure 2. Pt dissolution measured via gas diffusion electrode setup coupled to an inductively coupled plasma mass spectrometer (GDE-ICP-MS) in 0.1 M $HClO_4$. A–C) Pt dissolution profiles from Pt/C gas diffusion electrodes (HiSPEC 4000 on Freudenberg H23C8) with different loadings. A) Whole protocol, B) slow cycling at 10 mV s^{-1} between 0.1 and 1.5 V vs. RHE, C) fast cycling at 200 mV s^{-1} in the same potential range. D–F) Quantitative results for the Pt dissolution, respectively (E and F normalized per cycle). G) Qualitative comparison of 10 mV s^{-1} CVs before and after degradation cycles. H) Cross-sectional scanning electron microscope (SEM) images of the corresponding GDEs with different loadings.

relevant catalyst dissolution mechanism and that Pt is slightly stabilized after initial leaching of most energetic sites.

It has been discussed above that the catalyst–electrolyte interface and therefore the mass transport of Pt species plays a major role in Pt dissolution. To gain deeper insights into this phenomenon and further approach realistic fuel cell conditions, Nafion membranes in two different thicknesses were hot-pressed onto the GDEs. With this modification, it was possible to directly measure Pt dissolution in a polymer electrolyte environment and evaluate the mobility of dissolved Pt species in a membrane for the first time reported in the literature (Figure 3). The corresponding electrochemical data for these experiments can be found in Figures S9 and S10.

When comparing Pt dissolution in these different electrode–electrolyte interfaces, a reduction of Pt dissolution by a factor of approximately three can be observed when a Nafion membrane is added on top of the catalyst layer (Figure 3 A–F). The results are in good agreement with observations from early SEM experiments with Pt/WO_3[21] and more recent IL-TEM studies on Pt_3Co/C nanoparticles.[13] This phenomenon can again be explained by a higher transport resistivity for Pt ions in Nafion compared to aqueous electrolyte resulting in enhanced re-deposition of dissolved Pt species and a shift in the equilibrium dissolution potential. Another possible explanation could be that dissolved platinum species are stabilized in micro-cracks within the ionomer of the catalyst layer, as proposed in earlier works.[22] When the amount of dissolved Pt species is compared, the impact of membrane thickness seems to play a minor role (Figure 3 D–F). However, qualitatively some differences can be detected in the dissolution profiles. When fast degradation cycles are conducted, a shift in the dissolution onset is visible when membranes are added on top of the catalyst layer (Figure 3 C). This becomes even more explicit when dissolution profiles at slow CVs are compared (Figure 3 G). A clear peak tailing with thicker membrane can be detected in these dissolution profiles (Figure 3 G). This tailing is confirmed in potentiostatic hold experiments (Figure 3 H), where shifts in peak onset and the position of the peak maximum can be detected as well as a general tailing of the dissolution peaks after the maximum when different membranes are added on top of the catalyst layer. This effect can be attributed to the slower Pt diffusion through a membrane compared to the electrolyte and is logically more pronounced for the thicker membrane.

To attain a more profound understanding of the Pt diffusion in Nafion membranes, various membrane thicknesses have been spray coated onto a Pt film sputtered onto a Si wafer, and dissolution behavior was tested in an SFC setup. The results are displayed in Figure S11. In accordance with the results obtained from GDE-ICP-MS, a clear peak tailing can be observed when membranes are added on top of the catalyst layer (Figure S9A). Similar to GDE-ICP-MS experiments, it is more pronounced with increasing membrane thickness because the diffusion pathway for dissolved

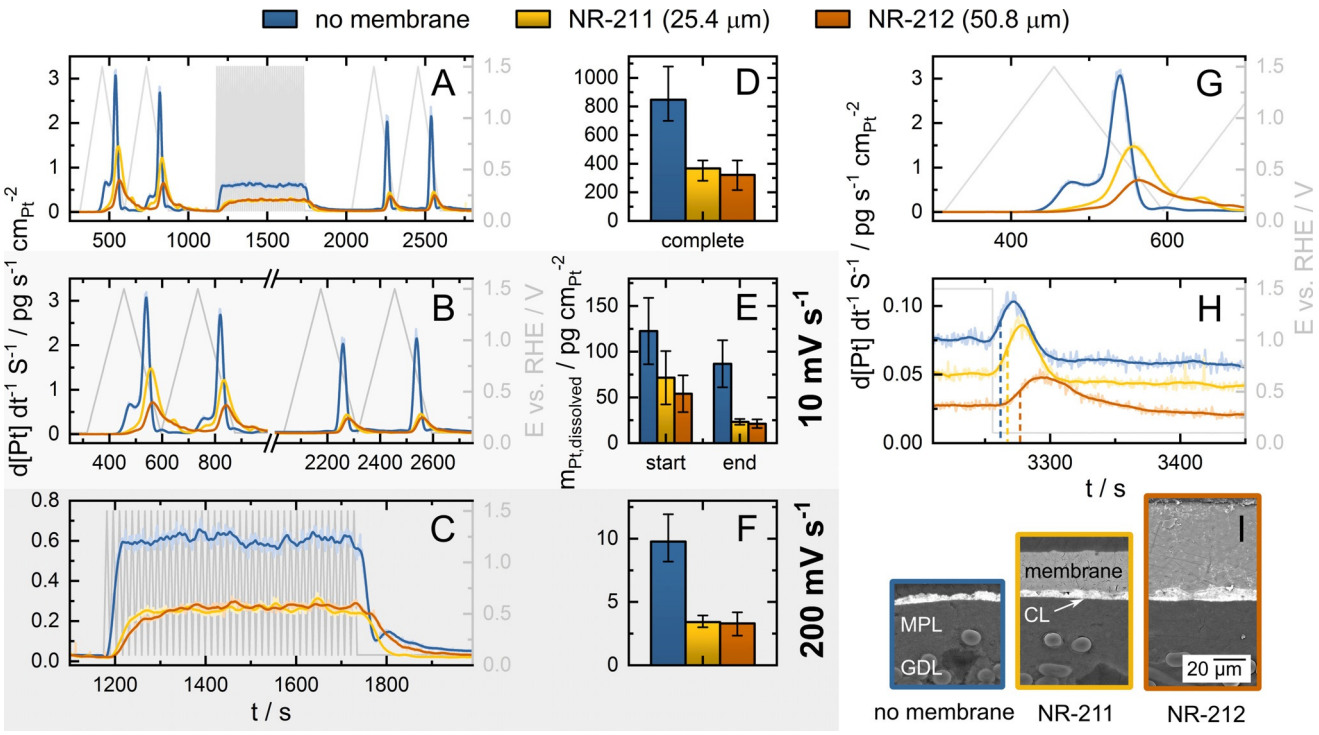

Figure 3. Pt dissolution measured via gas diffusion electrode setup coupled to an inductively coupled plasma mass spectrometer (GDE-ICP-MS) in 0.1 M $HClO_4$. A–C) Pt dissolution profiles from Pt/C gas diffusion electrodes (0.12 $mg_{Pt}\,cm^{-2}$, HiSPEC 4000 on Freudenberg H23C8) without membrane (blue) compared to similar samples with hot-pressed Nafion membranes of two different thicknesses (yellow: NR-211, 25.4 µm; orange: NR-212, 50.8 µm). A) Whole protocol, B) slow cycling at 10 $mV\,s^{-1}$ between 0.1 and 1.5 V vs. RHE, C) fast cycling at 200 $mV\,s^{-1}$ in the same potential range. D–F) Quantitative results for the Pt dissolution, respectively (E and F normalized per cycle). G) Qualitative comparison of the first CV with 10 $mV\,s^{-1}$. H) Comparison of peak tailing with potentiostatic hold, I) cross-sectional scanning electron microscope (SEM) images of the corresponding GDEs with different membrane thickness.

Pt species is extended. To further investigate Pt transport mechanisms within the membrane, the time shift induced by the membrane was quantified using potentiostatic hold experiments. After that, the time when dissolution signal hits the half the total peak height after a reductive step from 1.5 V vs. RHE to 0.1 V vs. RHE was compared (Figure 3H, dashed lines). This membrane induced shift in the dissolution peak from SFC and GDE experiments is compared to modeling results in Figure 4.

To be sure, to consider transport mechanisms only within the membrane and not at the membrane-electrode interface, the time shift of the dissolution response was always referred to the sample with the thinnest membrane ($x_{min,SFC} = 5$ µm and $x_{min,GDE} = 25.4$ µm). Figure 4 shows an excellent agreement between results obtained from SFC and GDE-ICP-MS experiments. This indicates on the one hand side that the different membrane structures (spray coated membrane in SFC and commercial membrane hot-pressed onto the catalyst layer in GDE experiments) do not have a significant impact on the mobility of Pt species within Nafion. On the other hand, it again proves the suitability of the newly established GDE-ICP-MS approach for online catalyst dissolution studies. When those experimental values are compared to numerical modeling results, a diffusion coefficient of around $4 \times 10^{-11}\ m^2\,s^{-1}$ can be determined. To the best of our knowledge, this is the first experimental determination of the diffusion coefficient of dissolved Pt species in a Nafion

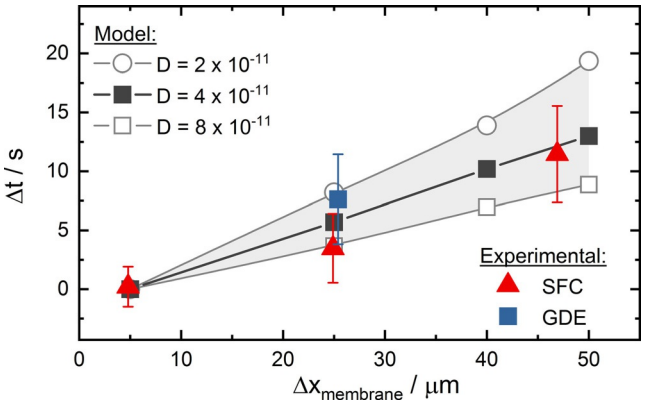

Figure 4. Membrane-induced time-shift of the dissolution response on reductive step (1.5 to 0.1 V vs. RHE) measured in scanning flow cell (SFC) (red) and GDE-ICP-MS (blue) in comparison to the modeled time delay for two different values of D in $m^2\,s^{-1}$ (gray).

membrane. The diffusion coefficient determined in our online ICP-MS experiments is well in line with the assumed or calculated data in the literature (Table 1).

It has to be stated that diffusion coefficients of dissolved Pt species are mostly assumed,[24] roughly calculated[25] or fitted to match experimental single cell degradation data to degradation models.[26,29] The values range from

Table 1: Comparison of different diffusion coefficients stated in literature.

D [$\times 10^{-11}$ m^2 s^{-1}]	Method	Comments on the method	Reference
0.18	Experimental	Permeation experiments with $PtCl_6^{2-}$ in Nafion 117	Kang 1999[23]
10	Theoretical	Assumed arbitrarily to be a factor of 10 lower than in water	Darling 2005[24]
8	Theoretical	Mobility of Pt^{2+} in the ionomer derived from calculation, based on the Pt-ion mobility in water and the volume fraction of ionomer etc.	Ferreira 2005[25]
0.015	Theoretical	Model first run with assumed value from ref. 24 but did adjust to match experimental degradation data.	Bi 2008[26]
7	Theoretical	Assumption diffusion coefficient is the same for all doubly ionized aqueous metal cations: $D_{Pt^{2+}\,Pt2+} \approx D_{Cu^{2+}}$, $D_{Cu^{2+}}$ from [27]	Holby 2012[28]
0.1	Theoretical	Value calibrated to their model using experimental data with Nafion NR-212 membrane.	Barrici 2018[29]
4	Experimental	Measured via online ICP-MS	This work

0.015×10^{-11} m^2 s^{-1} to 10×10^{-11} m^2 s^{-1}. Hitherto, experimental studies have only been conducted with either $PtCl_6^{2-}$ [23] or various bivalent metal cations[30] in fully hydrated Nafion 117 membrane. From the latter, diffusion coefficients for Ba ($D_{Ba^{2+}}$: 1.46×10^{-11} m^2 s^{-1})[30a] and Cu ions ($D_{Cu^{2+}}$: 2.9×10^{-11} m^2 s^{-1})[30b] have been measured. Those values for bivalent cations are in good agreement with the diffusion coefficient of Pt species determined experimentally in this study. However, it has to be stated that the diffusion coefficients determined in all these studies (including the present) display the diffusion of Pt species within a fully hydrated Nafion membrane. In real fuel cell devices, also lower membrane hydration states with probably lower mobility of Pt species could arise.

The diffusion coefficient of Pt ions in water ($D = 1 \times 10^{-9}$ m^2 s^{-1} [27]) is about one order of magnitude higher compared to Nafion. Therefore, the mobility of Pt in aqueous media is significantly enhanced in aqueous electrolyte compared to Nafion. As discussed above, the change in Pt mobility affects overall Pt dissolution drastically. This effect leads to significant changes in measured dissolution in aqueous model (SFC, RDE) and GDE systems as displayed in Figure 5. Here total Pt dissolution in GDE setup and model SFC system[6c,11] is compared and proposed transport mechanisms in both systems are depicted.

The comparison reveals that the relative trend of the impact of catalyst loading on Pt dissolution is consistent between dissolution data from GDE and previously reported data from model systems measured in an SFC with flowing electrolyte.[6c,11] However, the studies in the GDE-ICP-MS setup reveal lower total dissolution rates of about one order of magnitude. This can mainly be attributed to the difference in the catalyst–electrolyte interface of the two systems, affecting—as discussed—the mobility of dissolved Pt species and therefore re-deposition and equilibrium potential. In SFC experiments with model catalyst layers, the catalyst layer is completely flooded (Figure 5, top). Hence, Pt nanoparticles are in direct contact with acidic aqueous media. However, in GDE experiments, the catalyst is not completely flooded (Figure 5, bottom) as was shown in previous half-cell experiments by achieving oxygen reduction reaction (ORR) current densities of up to 2 A cm^{-2}.[15b,d,16] Thus, dissolved Pt species can only be transported out of the catalyst layer into the liquid electrolyte via the ionomer. As the mobility of Pt species in ionomer is about one order of magnitude lower compared to

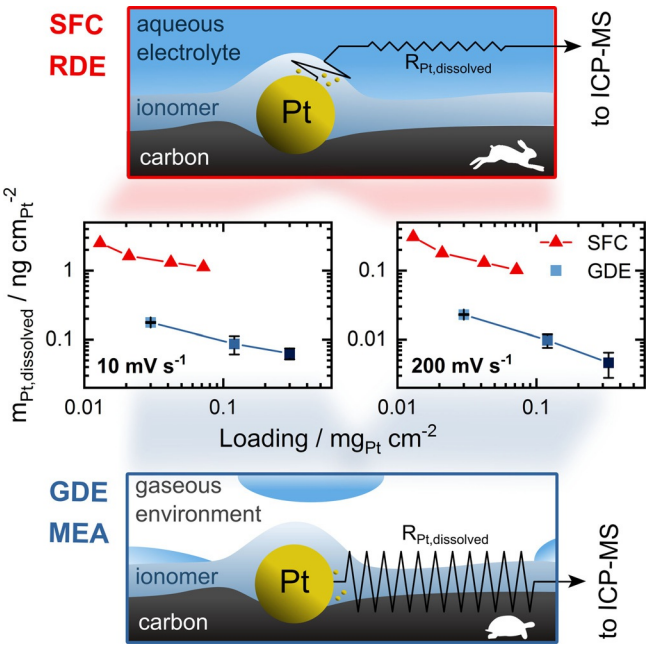

Figure 5. Comparison of Pt dissolution in GDE (this work) and model system (scanning flow cell (SFC), data extracted from [6c, 11]). The difference in Pt dissolution can be explained by the varying mass transport in model systems (RDE, SFC) with flooded catalyst layer (top) and realistic catalyst layers (GDE, MEA, bottom).

acidic media (see preceding discussion), it leads to increased re-deposition and a shift in the equilibrium potential in GDE or MEA setups compared to model systems.

Unfortunately, a direct comparison between catalyst dissolution in SFC or GDE-ICP-MS and a real fuel cell is impossible as there is no dissolution data for single cell experiments. Yet, dissolution in an SFC system has been compared to dissolution in a PEM electrolyzer. This comparison revealed a drastically higher dissolution of Ir for the SFC model system.[14] Besides possible differences in local pH, this was mainly attributed to transport phenomena in realistic catalyst layers in single cells. We therefore suggest that the GDE-ICP-MS setup with its realistic catalyst layer should mimic a real device—with its solid electrolyte—better compared to flow cell experiments. Additionally, this novel technique opens up opportunities to unravel catalyst degradation phenomena which cannot be investigated completely

in aqueous model systems due to their mass-transport limitations (e.g. enhanced non-precious catalyst degradation in presence of O_2[31]). However, to further approach realistic fuel cell conditions, the elevated temperature in fuel cell applications needs to be considered as this leads to significant increase of catalyst degradation.[32]

In general, it has to be stated that GDE half-cell experiments offer unique opportunities to study catalyst layers and their degradation by combining them with different analytical methods such as identical location transmission electron microscopy (IL-TEM),[33] operando X-ray and neutron imaging,[34] small-angle X-ray scattering (SAXS),[35] mass spectrometry for gaseous and volatile products,[36] and with the present work also ICP-MS.

Conclusion

For the first time reported in the literature, both Pt dissolution in realistic catalyst layers and the mobility of dissolved Pt species in Nafion membranes were evaluated directly by coupling a GDE half-cell to an ICP-MS. With this novel method, it was possible to close the gap between fundamental catalyst dissolution studies and real device degradation behavior. The impact of catalyst loading and the catalyst–electrolyte interface on Pt dissolution were successfully investigated. Thereby, the following insights were obtained: 1) specific Pt dissolution increased drastically with lower Pt loading, revealing the need for stabilization or mitigation strategies for Pt dissolution when aiming at low loading PEMFC. 2) Compared to experiments on model systems with flow cells, the measured dissolution in realistic GDE catalyst layers was about one order of magnitude lower. 3) By adding a Nafion membrane on top of the catalyst layer, Pt dissolution was reduced by a factor of three. All those phenomena can be explained by the fact that impeded mass transport of dissolved Pt species away from the catalytic centers results in decreased net dissolution due to redeposition and a shift in equilibrium potential. These results reveal the importance of Pt mass transport on Pt dissolution. To gain deeper insights into the mass transport of Pt species in Nafion, SFC experiments using different membrane thicknesses were conducted. In combination with numerical calculations, the diffusion coefficient of dissolved Pt ions in fully hydrated Nafion membranes was determined as $4 \times 10^{-11}\ m^2 s^{-1}$, which is more than one order of magnitude lower compared to the diffusion of Pt species in aqueous electrolyte. This difference between Pt mass transport in aqueous media of fully flooded model catalyst layer and ionomer in realistic catalyst layers explains the distinct degradation rates in experiments conducted in aqueous flow cells and real devices. In general, it can be concluded that GDE half-cell experiments offer unique opportunities to study catalyst layers and their degradation by coupling them directly to analytical methods. These opportunities will contribute significantly to bridge the gap between fundamental and applied fuel cell degradation studies.

Acknowledgements

K.E. acknowledges the Heinrich Böll Foundation for financial support, Florian D. Speck and Mario Löffler for valuable scientific discussions and Achim Mannke, Stefan Borlein, Stefan Fiegl and Jonas Möller for technical support. The authors thank Olga Kasian for sputtering Pt films for SFC experiments. This work was supported by the German Federal Ministry for Economic Affairs and Energy (grant number 03ETBO27A). Open access funding enabled and organized by Projekt DEAL.

Conflict of interest

The authors declare no conflict of interest.

Keywords: catalyst degradation · electrochemistry · gas diffusion electrodes · Nafion · Pt dissolution

[1] T. Yoshida, K. Kojima, *Electrochem. Soc. Interface* **2015**, *24*, 45–49.

[2] R. L. Borup, A. Kusoglu, K. C. Neyerlin, R. Mukundan, R. K. Ahluwalia, D. A. Cullen, K. L. More, A. Z. Weber, D. J. Myers, *Curr. Opin. Electrochem.* **2020**, *21*, 192–200.

[3] a) R. Borup, J. Meyers, B. Pivovar, Y. S. Kim, R. Mukundan, N. Garland, D. Myers, M. Wilson, F. Garzon, D. Wood, P. Zelenay, K. More, K. Stroh, T. Zawodzinski, J. Boncella, J. E. McGrath, M. Inaba, K. Miyatake, M. Hori, K. Ota, Z. Ogumi, S. Miyata, A. Nishikata, Z. Siroma, Y. Uchimoto, K. Yasuda, K.-i. Kimijima, N. Iwashita, *Chem. Rev.* **2007**, *107*, 3904–3951; b) J. C. Meier, C. Galeano, I. Katsounaros, J. Witte, H. J. Bongard, A. A. Topalov, C. Baldizzone, S. Mezzavilla, F. Schüth, K. J. J. Mayrhofer, *Beilstein J. Nanotechnol.* **2014**, *5*, 44–67; c) L. Dubau, L. Castanheira, F. Maillard, M. Chatenet, O. Lottin, G. Maranzana, J. Dillet, A. Lamibrac, J. C. Perrin, E. Moukheiber, A. El Kaddouri, G. D. Moor, C. Bas, L. Flandin, N. Caqué, *Wiley Interdiscip. Rev. Energy Environ.* **2014**, *3*, 540–560.

[4] a) S. Mezzavilla, S. Cherevko, C. Baldizzone, E. Pizzutilo, G. Polymeros, K. J. J. Mayrhofer, *ChemElectroChem* **2016**, *3*, 1524–1536; b) N. Hodnik, S. Cherevko, *Curr. Opin. Electrochem.* **2019**, *15*, 73–82.

[5] a) J. A. Gilbert, N. N. Kariuki, X. Wang, A. J. Kropf, K. Yu, D. J. Groom, P. J. Ferreira, D. Morgan, D. J. Myers, *Electrochim. Acta* **2015**, *173*, 223–234; b) C. Lafforgue, M. Chatenet, L. Dubau, D. R. Dekel, *ACS Catal.* **2018**, *8*, 1278–1286.

[6] a) R. Lin, X. Cai, H. Zeng, Z. Yu, *Adv. Mater.* **2018**, *30*, 1705332; b) S. Cherevko, N. Kulyk, K. J. J. Mayrhofer, *Nano Energy* **2016**, *29*, 275–298; c) S. Cherevko, *Curr. Opin. Electrochem.* **2018**, *8*, 118–125.

[7] a) K. Ogle, S. Weber, *J. Electrochem. Soc.* **2000**, *147*, 1770–1780; b) S. O. Klemm, A. A. Topalov, C. A. Laska, K. J. J. Mayrhofer, *Electrochem. Commun.* **2011**, *13*, 1533–1535; c) A. A. Topalov, S. Cherevko, A. R. Zeradjanin, J. C. Meier, I. Katsounaros, K. J. J. Mayrhofer, *Chem. Sci.* **2014**, *5*, 631–638; d) P. Jovanovič, A. Pavlišič, V. S. Šelih, M. Šala, N. Hodnik, M. Bele, S. Hočevar, M. Gaberščček, *ChemCatChem* **2014**, *6*, 449–453; e) A. Pavlišič, P. Jovanovič, V. S. Šelih, M. Šala, N. Hodnik, S. Hočevar, M. Gaberščček, *Chem. Commun.* **2014**, *50*, 3732–3734; f) P. P. Lopes, D. Strmcnik, D. Tripkovic, J. G. Connell, V. Stamenkovic, N. M. Markovic, *ACS Catal.* **2016**, *6*, 2536–2544; g) R. K. Ahluwalia, D. D. Papadias, N. N. Kariuki, J.-K. Peng, X. Wang, Y. Tsai, D. G. Graczyk, D. J. Myers, *J. Electrochem. Soc.* **2018**, *165*, F3024–F3035.

[8] O. Kasian, S. Geiger, K. J. J. Mayrhofer, S. Cherevko, *Chem. Rec.* **2019**, *19*, 2130 – 2142.
[9] A. Pavlišič, P. Jovanovič, V. S. Šelih, M. Šala, N. Hodnik, M. Gaberšček, *J. Electrochem. Soc.* **2018**, *165*, F3161 – F3165.
[10] T. Nagai, H. Murata, Y. Morimoto, *ECS Trans.* **2013**, *50*, 1539 – 1545.
[11] G. P. Keeley, S. Cherevko, K. J. J. Mayrhofer, *ChemElectroChem* **2016**, *3*, 51 – 54.
[12] a) Y.-H. Cho, J. W. Lim, Y. S. Kang, Y.-H. Cho, O.-H. Kim, N.-H. Kwon, O. J. Kwon, W.-S. Yoon, H. Choe, Y.-E. Sung, *Int. J. Hydrogen Energy* **2012**, *37*, 2490 – 2497; b) P. Gazdzicki, J. Mitzel, A. M. Dreizler, M. Schulze, K. A. Friedrich, *Fuel Cells* **2018**, *18*, 270 – 278.
[13] F. R. Nikkuni, B. Vion-Dury, L. Dubau, F. Maillard, E. A. Ticianelli, M. Chatenet, *Appl. Catal. B* **2014**, *156 – 157*, 301 – 306.
[14] S. Geiger, O. Kasian, M. Ledendecker, E. Pizzutilo, A. M. Mingers, W. T. Fu, O. Diaz-Morales, Z. Li, T. Oellers, L. Fruchter, A. Ludwig, K. J. J. Mayrhofer, M. T. M. Koper, S. Cherevko, *Nat. Catal.* **2018**, *1*, 508 – 515.
[15] a) C. M. Zalitis, D. Kramer, A. R. Kucernak, *Phys. Chem. Chem. Phys.* **2013**, *15*, 4329 – 4340; b) B. A. Pinaud, A. Bonakdarpour, L. Daniel, J. Sharman, D. P. Wilkinson, *J. Electrochem. Soc.* **2017**, *164*, F321 – F327; c) M. Inaba, A. W. Jensen, G. W. Sievers, M. Escudero-Escribano, A. Zana, M. Arenz, *Energy Environ. Sci.* **2018**, *11*, 988 – 994; d) K. Ehelebe, D. Seeberger, M. T. Y. Paul, S. Thiele, K. J. J. Mayrhofer, S. Cherevko, *J. Electrochem. Soc.* **2019**, *166*, F1259 – F1268.
[16] K. Ehelebe, T. Ashraf, S. Hager, D. Seeberger, S. Thiele, S. Cherevko, *Electrochem. Commun.* **2020**, *116*, 106761.
[17] D. J. S. Sandbeck, N. M. Secher, M. Inaba, J. Quinson, J. E. Sørensen, J. Kibsgaard, A. Zana, F. Bizzotto, F. D. Speck, M. T. Y. Paul, A. Dworzak, C. Dosche, M. Oezaslan, I. Chorkendorff, M. Arenz, S. Cherevko, *J. Electrochem. Soc.* **2020**, *167*, 164501.
[18] a) S. Cherevko, A. R. Zeradjanin, A. A. Topalov, N. Kulyk, I. Katsounaros, K. J. J. Mayrhofer, *ChemCatChem* **2014**, *6*, 2219 – 2223; b) P. P. Lopes, D. Li, H. Lv, C. Wang, D. Tripkovic, Y. Zhu, R. Schimmenti, H. Daimon, Y. Kang, J. Snyder, N. Becknell, K. L. More, D. Strmcnik, N. M. Markovic, M. Mavrikakis, V. R. Stamenkovic, *Nat. Mater.* **2020**, *19*, 1207 – 1214.
[19] S. Cherevko, A. R. Zeradjanin, G. P. Keeley, K. J. J. Mayrhofer, *J. Electrochem. Soc.* **2014**, *161*, H822 – H830.
[20] Y. Yu, H. Li, H. Wang, X.-Z. Yuan, G. Wang, M. Pan, *J. Power Sources* **2012**, *205*, 10 – 23.
[21] K. Y. Chen, A. C. C. Tseung, *J. Electrochem. Soc.* **1996**, *143*, 2703 – 2707.
[22] a) S. Takao, O. Sekizawa, S.-i. Nagamatsu, T. Kaneko, T. Yamamoto, G. Samjeské, K. Higashi, K. Nagasawa, T. Tsuji, M. Suzuki, N. Kawamura, M. Mizumaki, T. Uruga, Y. Iwasawa, *Angew. Chem. Int. Ed.* **2014**, *53*, 14110 – 14114; *Angew. Chem.* **2014**, *126*, 14334 – 14338; b) S. Takao, O. Sekizawa, G. Samjeské, S.-i. Nagamatsu, T. Kaneko, T. Yamamoto, K. Higashi, K. Nagasawa, T. Uruga, Y. Iwasawa, *J. Phys. Chem. Lett.* **2015**, *6*, 2121 – 2126.
[23] M. S. Kang, Y. I. Joe, *J. Power Sources* **1999**, *77*, 49 – 55.
[24] R. M. Darling, J. P. Meyers, *J. Electrochem. Soc.* **2005**, *152*, A242 – A247.
[25] P. J. Ferreira, G. J. la O', Y. Shao-Horn, D. Morgan, R. Makharia, S. Kocha, H. A. Gasteiger, *J. Electrochem. Soc.* **2005**, *152*, A2256 – A2271.
[26] W. Bi, T. F. Fuller, *J. Power Sources* **2008**, *178*, 188 – 196.
[27] J. Newman, K. E. Thomas-Alyea, *Electrochemical Systems*, Wiley, Hoboken, **2012**.
[28] E. F. Holby, D. Morgan, *J. Electrochem. Soc.* **2012**, *159*, B578 – B591.
[29] A. Baricci, M. Bonanomi, H. Yu, L. Guetaz, R. Maric, A. Casalegno, *J. Power Sources* **2018**, *405*, 89 – 100.
[30] a) A. Goswami, A. Acharya, A. K. Pandey, *J. Phys. Chem. B* **2001**, *105*, 9196 – 9201; b) G. Suresh, Y. M. Scindia, A. K. Pandey, A. Goswami, *J. Phys. Chem. B* **2004**, *108*, 4104 – 4110.
[31] a) F. D. Speck, P. G. Santori, F. Jaouen, S. Cherevko, *J. Phys. Chem. C* **2019**, *123*, 25267 – 25277; b) K. Kumar, L. Dubau, M. Mermoux, J. Li, A. Zitolo, J. Nelayah, F. Jaouen, F. Maillard, *Angew. Chem. Int. Ed.* **2020**, *59*, 3235 – 3243; *Angew. Chem.* **2020**, *132*, 3261 – 3269.
[32] a) L. Dubau, F. Maillard, *Electrochem. Commun.* **2016**, *63*, 65 – 69; b) L. Dubau, M. Lopez-Haro, J. Durst, F. Maillard, *Catal. Today* **2016**, *262*, 146 – 154; c) G. Polymeros, C. Baldizzone, S. Geiger, J. P. Grote, J. Knossalla, S. Mezzavilla, G. P. Keeley, S. Cherevko, A. R. Zeradjanin, F. Schüth, K. J. J. Mayrhofer, *Electrochim. Acta* **2016**, *211*, 744 – 753; d) N. Maselj, M. Gatalo, F. Ruiz-Zepeda, A. Kregar, P. Jovanovič, N. Hodnik, M. Gaberšček, *J. Electrochem. Soc.* **2020**, *167*, 114506.
[33] S. Alinejad, M. Inaba, J. Schröder, J. Du, J. Quinson, A. Zana, M. Arenz, *J. Phys. Energy* **2020**, *2*, 024993.
[34] M. Gebhard, M. Paulisch, A. Hilger, D. Franzen, B. Ellendorff, T. Turek, I. Manke, C. Roth, *Materials* **2019**, *12*, 1275.
[35] J. Schröder, J. Quinson, J. K. Mathiesen, J. J. K. Kirkensgaard, S. Alinejad, V. A. Mints, K. Jensen, M. Ø. M. Arenz, *J. Electrochem. Soc.* **2020**, *167*, 134515.
[36] a) G. Zhang, A. Kucernak, *ACS Catal.* **2020**, *10*, 9684 – 9693; b) B. Hasa, M. Jouny, B. H. Ko, B. Xu, F. Jiao, *Angew. Chem. Int. Ed.* **2021**, *60*, 3277 – 3282.

Manuscript received: November 3, 2020
Revised manuscript received: December 15, 2020
Accepted manuscript online: January 6, 2021
Version of record online: March 9, 2021

